

# Reductive Reaction Mechanisms of the Azo Dye Orange II in Aqueous Solution and in Cellulose: From Radical Intermediates to Products

Laurence C. Abbott,<sup>†</sup> Stephen N. Batchelor,<sup>\*,‡</sup> John R. Lindsay Smith,<sup>†</sup> and John N. Moore<sup>\*,†</sup>

Department of Chemistry, The University of York, Heslington, York, YO10 5DD, U.K., and Unilever Research, Port Sunlight, Quarry Road East, Bebington, Wirral, CH63 3JW, U.K.

Received: March 9, 2009

Reductive reaction mechanisms of the azo dye Orange II (Acid Orange 7) in aqueous solution have been studied from radical intermediates through to the final products using a combination of nanosecond time-resolved UV–visible absorption spectroscopy, steady-state photolysis, and HPLC techniques. The dye is reduced by photochemically produced 2-hydroxy-2-propyl radicals at a near-diffusion-controlled rate ( $k_2 = 2.2 \times 10^9 \text{ dm}^3 \text{ mol}^{-1} \text{ s}^{-1}$ ) to give the dye radical anion, which then disproportionates ( $k_3 = 2.6 \times 10^8 \text{ dm}^3 \text{ mol}^{-1} \text{ s}^{-1}$ ) to re-form the parent dye and a hydrazine. The hydrazine decomposes to 4-aminobenzenesulfonate and a naphthylimine species, which hydrolyses to give 1,2-naphthoquinone; this naphthoquinone and 4-aminobenzenesulfonate react to give a species that reacts further in the presence of air to form an indophenol dye. The reduction of Orange II has also been studied in cellophane, where the rate constant for dye reduction by 2-hydroxy-2-propyl radicals is approximately two orders of magnitude lower than that in aqueous solution.

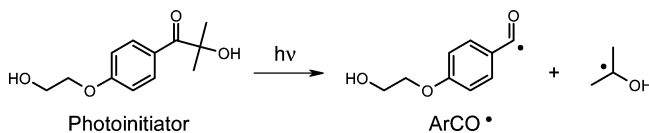
## Introduction

Azo dyes are the largest class of dyes produced globally, and they are used widely in industries ranging from food additives, pharmaceuticals, and cosmetics to textiles and printing. It is important to have a good knowledge of the degradation pathways of the dyes, for example, to understand the unwanted fading of dyed goods or the efficient degradation required in treating effluent from textile dyeing plants.<sup>1</sup> Detailed mechanistic information is also important in understanding large changes in stability that can result from relatively minor structural changes between dyes, and in identifying the routes to final products. Oxidation and reduction both provide important degradation routes for azo dyes, and they can be induced under various conditions by photolysis,<sup>2–6</sup> electrolysis,<sup>2,7–10</sup> radiolysis,<sup>11–13</sup> bacteria,<sup>14–17</sup> or chemical reagents.<sup>18–22</sup> Oxidation reactions may dominate under air but reduction reactions compete and may dominate under anaerobic conditions, with cleavage of the azo group being an important reductive degradation pathway; reduction is a key metabolic pathway in mammals, and the products are key to the toxicology of dyes.<sup>23</sup>

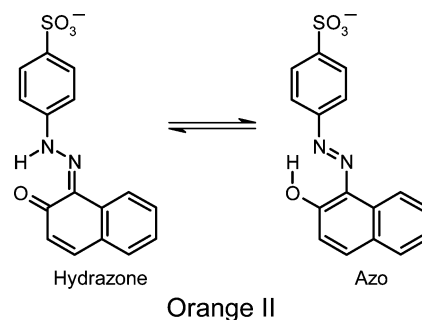
It is well established that irradiation of cellulosic substrates, such as cotton and cellophane, gives rise to relatively long-lived free radicals, such as  $\alpha$ -hydroxyalkyl radicals,<sup>24–26</sup> that can initiate the reductive degradation of dyes. Recent time-resolved studies have shown that  $\alpha$ -hydroxyalkyl radicals produced by photolysis or radiolysis of various precursors can induce the one-electron reduction of azo dyes at near-diffusion-controlled rates in solution<sup>5,27,28</sup> and on cotton.<sup>29</sup> The formation and decay of azo dye radical species has been observed directly in real time, and simple monoazo dye radicals have been reported to decay by second-order disproportionation reactions.<sup>30,31</sup>

The monoazo dye Orange II (Acid Orange 7; shown below) has been widely studied as a model because it has a simpler structure than many industrially important dyes, and it is known to exist principally as the hydrazone tautomer in aqueous

## SCHEME 1: Photolysis of Photoinitiator



solution.<sup>32</sup> Orange II degrades under both reductive and oxidative conditions, and reports have included time-resolved studies that have focused mainly on radical formation reactions<sup>27,33–35</sup> and HPLC studies that have identified final degradation products under various conditions.<sup>4,13,15,17</sup>



We recently studied the structure and bonding of radicals produced on reduction of Orange II by chemically produced 2-hydroxy-2-propyl radicals, using electron paramagnetic resonance (EPR) spectroscopy allied with density functional theory (DFT) calculations.<sup>32</sup> Here, we report mechanistic studies of Orange II reduction. Our principal aims were to observe the formation and decay of the dye radical anion, to deduce the radical reaction mechanisms including rate constants, and to determine an overall reaction scheme including final products. The one-electron reduction of Orange II has been induced by 2-hydroxy-2-propyl radicals produced on photolysis of a photoinitiator (Scheme 1),<sup>36</sup> which also gives benzoyl radicals

<sup>†</sup> The University of York.

<sup>‡</sup> Unilever Research.

(ArCO<sup>\*</sup>) that do not provide a major route to dye degradation under the conditions used here. Nanosecond time-resolved UV–visible (TRVIS) spectroscopy has been used to study the radical reactions in real time, and steady-state studies with UV–visible monitoring and HPLC analysis have been used to identify the reaction products. We report the reduction of Orange II first in aqueous solution, including a brief spectroelectrochemical study, and second in cellophane to observe reduction in a cellulosic environment that may mimic that of paper and cotton.<sup>37</sup>

## Experimental Section

**Materials.** Orange II (Aldrich) and the photoinitiator 2-hydroxy-4'-(2-hydroxyethoxy)-2-methylpropiophenone (Irgacure 2959, Ciba Specialty Chemicals) were used as received and were found to be pure by NMR; 4-aminobenzenesulfonic acid, 1,2-naphthoquinone, and 1-amino-2-naphthol hydrochloride (all Aldrich), methanol, acetonitrile, KCl, and ammonium acetate (all Fisher Scientific), and freshly deionized water were used as received. Cellophane samples were prepared by soaking small (ca. 6 × 2 cm) pieces of cellophane film (Sigma; thickness 45 μm) in solution for ca. 30 min and drying them between lint-free tissues with a weight on top to prevent wrinkling. Solutions used to prepare cellophane samples were an aqueous solution of dye at ca. 3 × 10<sup>-3</sup> mol dm<sup>-3</sup> (dye only), a methanol solution of photoinitiator at 0.1 mol dm<sup>-3</sup> (photoinitiator only), and 50:50 water:methanol solutions of dye at (1–5) × 10<sup>-3</sup> mol dm<sup>-3</sup> and photoinitiator at 0.05 mol dm<sup>-3</sup> (dye + photoinitiator). Concentrations in cellophane samples were estimated by assuming that the peak absorption coefficients are the same as those in solution. The cellophane samples were placed between quartz microscope slides and the edges sealed with adhesive tape; wet cellophane samples were prepared by removing the sample from the dyeing solution and briefly rinsing it in water for ca. 1–2 s, to remove any excess dye solution, before sealing it between microscope slides.

**Steady-State Studies.** UV–visible absorption spectra were recorded using a spectrophotometer (Hitachi U-3010) with either 1 cm or 1 mm path length matched quartz cells (Hellma).

Spectroelectrochemical studies were performed using a cell comprising a ca. 2.1 × 0.9 cm Pt-gauze working electrode, a Pt-wire counter electrode, and a Ag-wire reference electrode connected to a potentiostat (Oxford Electrodes Control Unit). UV–visible spectra were recorded through the gauze of the working electrode, which was situated in a 1 mm path length glass cell. Solutions for electrochemical study were purged with N<sub>2</sub> before being transferred to the purged cell, which was then sealed under N<sub>2</sub>. The applied potential was changed in increments, and the sample was allowed to equilibrate for 10 min before recording a spectrum. Samples for HPLC analysis were prepared by carefully and slowly syringing ≤0.5 cm<sup>3</sup> from around the working electrode.

Steady-state photolysis studies were performed using pulses from a camera flashgun (Ricoh Speedlight 260P; Guide Number 26), which was held directly against the solution or cellophane samples placed horizontally on a sheet of aluminum foil; the solution samples were purged with N<sub>2</sub> and sealed in a 1 cm path length quartz cell fitted with a Teflon tap (Youngs). UV–visible spectra were recorded after each pulse.

**Nanosecond TRVIS Studies.** Nanosecond TRVIS studies were performed using 308 nm pulses from a XeCl excimer laser (Lambda Physik EMG-50; ca. 20 ns pulse width) and UV–visible detection was effected using a 250 W Xe arc lamp, monochromator and photomultiplier tube (Applied Photophysics Laser

Kinetic spectrometer fitted with a Hamamatsu R928 photomultiplier tube): cutoff filters were used to block second-order effects and also to block UV output from the arc lamp where appropriate. A digital storage oscilloscope (Tektronix TDS 520) was used to collect kinetic data before transfer to a PC for analysis; typically, the laser pulse energy was 10–15 mJ measured at the sample and the results from 16 laser shots were averaged. Dye-only solution samples were held in a sealed 2 mm path length quartz cell under air. Photoinitiator-only and dye + photoinitiator solutions were held in a single-pass flow system comprising a sample reservoir that was continually purged with N<sub>2</sub>, a peristaltic pump (Cole Parmer 7553-75 with 7518-00 head), a 1 mm path length quartz flow cell (Hellma), Tygon tubing (Cole Parmer), and a waste reservoir; the pump was switched off for data acquisition and was briefly run between each laser pulse such that each laser pulse encountered fresh sample. Concentrations for the solution TRVIS studies were, typically, Orange II at 1 × 10<sup>-4</sup> mol dm<sup>-3</sup> and photoinitiator at 1 × 10<sup>-3</sup> mol dm<sup>-3</sup> in water. Cellophane samples were kept wet with the parent solution and held between quartz microscope slides which had been sealed round the edge with adhesive tape. The cellophane samples were mounted on an *x-y-z* translation stage and were translated between laser pulses so that each encountered a fresh, unphotolysed area of the sample.

TRVIS difference spectra were generated point-by-point by averaging time windows of the kinetic traces recorded at different probe wavelengths. Exponential fitting was performed with SPSS (SPSS Inc.), and kinetic modeling was performed with custom-written software that gave numerical integration of the differential rate laws using a Runge–Kutta algorithm. The modeled kinetics were scaled from concentrations to changes in absorbance (Δ*A*) using the Beer–Lambert law and compared with the measured Δ*A* kinetics to determine a least-squares value. Least-squares minimization was performed using two methods: first, a stepwise variation of each fitted parameter in turn was used to explore wide areas of the error surface; second, a simplex algorithm<sup>38</sup> was used to refine to the global minimum from the set of values found using the stepwise fitting, and without constraining any fitted parameters. Initial fitting attempts using the simplex method alone showed that the error surface had many local minima and so the stepwise method was adopted as a first step to avoid optimizing the fitted parameters to a local minimum.

**HPLC Studies.** HPLC analysis was performed with a chromatograph (HP1090) fitted with a 4.6 mm diameter C<sub>18</sub> reverse-phase column (Phenomenex Spherclone) held at 40 °C and a UV–visible diode-array detector. A binary solvent system of an aqueous buffer (0.07 mol dm<sup>-3</sup> ammonium acetate in water; pH 5.2) and acetonitrile was used, with an initial ratio of 98:2 buffer:acetonitrile that was ramped to 60:40 over 25 min, and then back to 98:2 over 1 min, followed by a further 10 min at this composition to wash the column; the sample injection volume was 25 μL.

## Results and Discussion

The studies of aqueous solutions are presented first, followed by those of cellophane samples, with each section comprising both steady-state and TRVIS studies. The HPLC product studies of aqueous solutions are presented last.

**Spectroelectrochemical Studies in Solution.** Figure 1 shows UV–visible spectra of Orange II during electrochemical reduction under N<sub>2</sub>. The spectrum showed negligible changes until the applied potential reached ca. -0.6 V (versus Ag wire), after

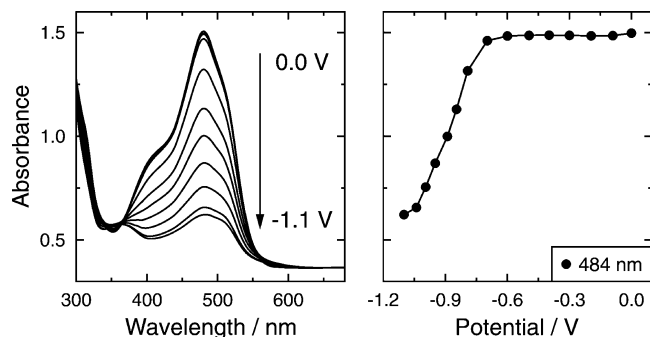


**Figure 1.** Left: UV-visible absorption spectra of Orange II ( $5 \times 10^{-4}$  mol dm<sup>-3</sup> in  $0.1$  mol dm<sup>-3</sup> KCl) recorded during electrochemical reduction under N<sub>2</sub>. Right: absorbance at 484 nm vs applied potential (relative to a Ag wire reference electrode).

which the main band showed a loss in absorbance (reaching ca. 20% of its initial value at  $-1.1$  V) as a new absorption feature at ca. 320–400 nm emerged along with the growth of a much weaker feature at ca.  $>550$  nm. Returning the applied potential to 0.0 V did not lead to a regrowth of the original spectrum, showing that Orange II undergoes irreversible chemical degradation on reduction. The applied potential required for the onset of reduction, and its irreversibility, are consistent with reported cyclic voltammetry studies of Orange II in aqueous solution that gave redox potentials of ca.  $-0.6$  V (versus Ag/AgCl) under slightly different conditions.<sup>14,39</sup>

**Steady-State Photolysis Studies in Solution.** Figure 2 shows steady-state UV-visible absorption spectra recorded during photolysis of aqueous solutions containing (a) Orange II alone, (b) photoinitiator alone, and (c) Orange II + photoinitiator, all under N<sub>2</sub>. Orange II alone showed negligible ( $<1\%$ ) fading after 20 flashgun pulses, whereas the photoinitiator alone showed a substantial and progressive decrease in the band at 279 nm, along with the simultaneous growth of features at ca. 330 and 240 nm. The Orange II + photoinitiator sample showed a large progressive decrease in the Orange II absorption band at 484 nm and, as it bleached fully, a band at 413 nm became prominent. This 413 nm band also decreased with further photolysis, but it showed only small changes over several days when the sample was kept in the dark under N<sub>2</sub>; however, a spectrum recorded immediately after exposing this sample to air showed that the 413 nm band had decreased and a new band at ca. 500 nm had formed, as shown in Figure 2d.

The spectral changes on photolysis of the samples containing photoinitiator are more clearly shown by the difference spectra in Figure 3a,b, which show the changes after the first flashgun pulse to emphasize the initial degradation of the dye and photoinitiator. The difference spectrum from the photoinitiator alone (Figure 3a) shows a negative feature at 273 nm that is blue-shifted by ca. 6 nm from the absorption band of the photoinitiator, suggesting that an overlying positive feature also contributes, along with positive features at 308 and 233 nm that arise from products. The difference spectrum from the Orange II + photoinitiator sample (Figure 3b, solid line) shows a large decrease in the main Orange II visible absorption band but the shoulder at ca. 410 nm observed from the reactant (Figure 2a) is not present in the bleaching feature, and its absence may be attributed to the overlying 413 nm band that became prominent with increasing photolysis (Figure 2c). In contrast, the overall difference spectrum from electrochemical reduction of Orange II alone (Figure 3c) shows that the whole of the visible absorption band has been bleached, including the shoulder at ca. 410 nm; this difference spectrum also shows the growth of weak new features at ca. 350 and 580 nm.

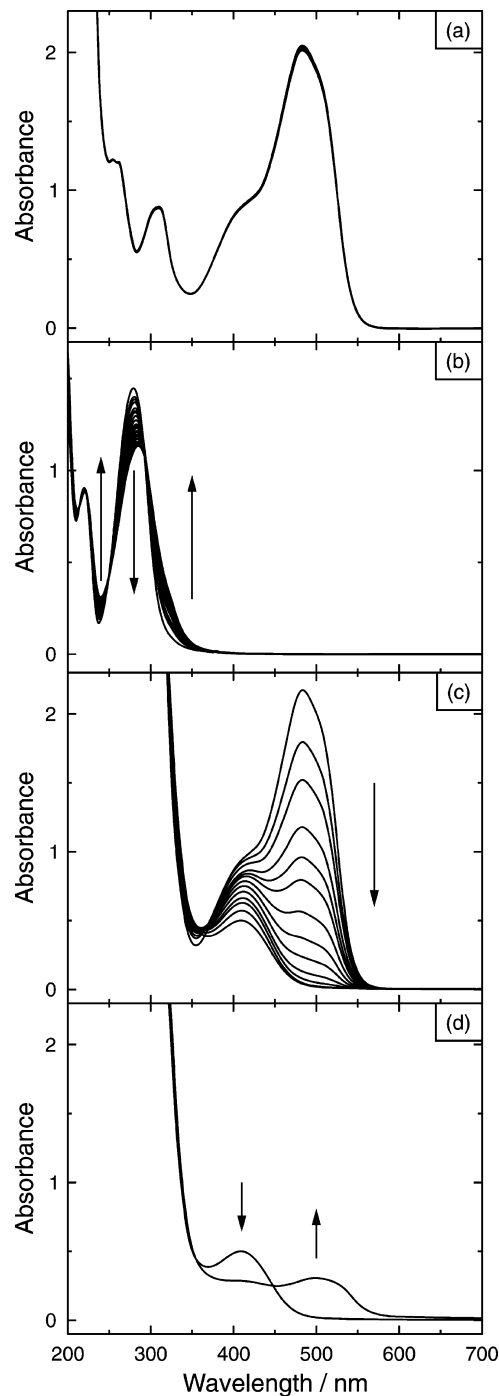


**Figure 2.** Steady-state UV-visible absorption spectra of (a) Orange II ( $1 \times 10^{-4}$  mol dm<sup>-3</sup>; 20 pulses), (b) photoinitiator ( $1 \times 10^{-4}$  mol dm<sup>-3</sup>; 20 pulses), and (c) Orange II and photoinitiator ( $1 \times 10^{-4}$  and  $1 \times 10^{-3}$  mol dm<sup>-3</sup>, respectively; 12 pulses), all recorded following flashgun photolysis in aqueous solution under N<sub>2</sub> and (d) the final sample from set (c), before and after exposure to air.

**TRVIS Studies of Photoinitiator Alone in Solution.** Figure 4 (top) shows TRVIS difference spectra and kinetics obtained on 308 nm photolysis of the photoinitiator alone in aqueous solution under N<sub>2</sub>. Transient absorption was observed at ca. 330–600 nm, comprising a main band at ca. 330–470 nm with a shoulder at longer wavelength; it rose within the instrument-response time ( $\leq 20$  ns) and decayed exponentially with a lifetime of  $\tau = 113 \pm 20$  ns to give a small residual absorption.

The photoinitiator studied here has been reported to show transient absorption attributed to the triplet state, with a band

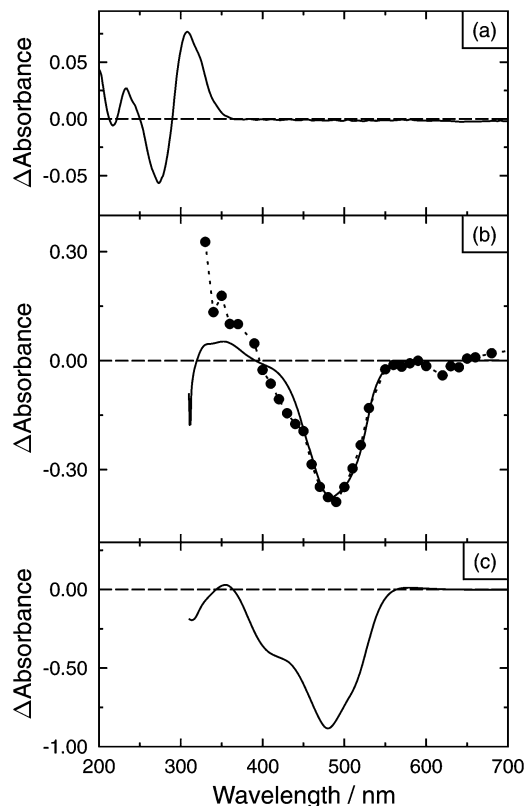


**Figure 3.** UV-visible difference spectra of (a) photoinitiator alone ( $1 \times 10^{-4}$  mol dm $^{-3}$ ) after one flashgun pulse, (b) Orange II + photoinitiator ( $1 \times 10^{-4}$  and  $1 \times 10^{-3}$  mol dm $^{-3}$ , respectively) after one flashgun pulse (solid line) along with a TRVIS difference spectrum at 3 ms after photolysis ( $\bullet$ ) scaled to give the same bleach magnitude for comparison, and (c) Orange II alone ( $5 \times 10^{-4}$  mol dm $^{-3}$ ) after electrochemical reduction to  $-1.1$  V; all samples under N $_2$ .

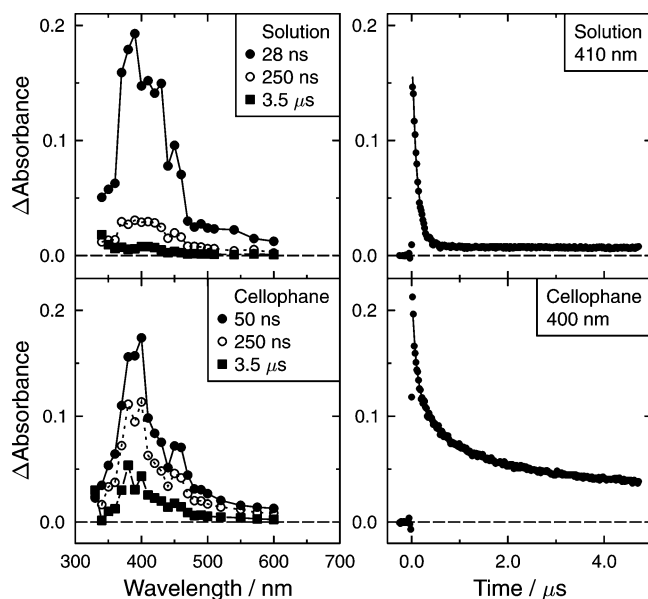


**Figure 4.** TRVIS difference spectra and kinetics of (top) photoinitiator alone in aqueous solution ( $1 \times 10^{-3}$  mol dm $^{-3}$ , under N $_2$ ) and (bottom) in cellophane ( $5 \times 10^{-2}$  mol dm $^{-3}$ ). Solid lines show single and biexponential fits to the kinetics for solution and cellophane samples, respectively.

at ca. 330–450 nm and a broad tail out to ca. 600 nm, and a lifetime of  $\tau = 11$  ns in acetonitrile that has been attributed to its cleavage to form the radicals shown in Scheme 1.<sup>36</sup> The similarity between the published difference spectra and those

in Figure 4 enable the transient absorption observed here to be assigned similarly to the photoinitiator triplet state, with our data indicating that its lifetime is longer (ca.  $\times 10$ ) in aqueous solution than that reported in acetonitrile. A significantly longer-lived species was also observed here, with a weak band at  $\lambda < 360$  nm that decayed with  $\tau \geq 0.5$  s, and which may have been the same species observed in the steady-state difference spectrum (Figure 3a).<sup>40</sup>

**TRVIS Studies of Orange II Alone in Solution.** Small TRVIS signals were observed on 308 nm photolysis of Orange II alone, with the use of relatively high laser energies and close inspection revealing weak bleaching at ca. 350–500 nm and weak transient absorption at ca. 600–650 nm; these TRVIS signals were not studied in detail, being much smaller than those observed from Orange II in the presence of photoinitiator that were the main focus of our work. UV-visible spectra recorded before and after the TRVIS experiments showed negligible ( $\ll 1\%$ ) sample loss, consistent with the small loss on steady-state photolysis of Orange II alone (Figure 2a).

**TRVIS Studies of Orange II + Photoinitiator in Solution.** Figure 5 (top) shows TRVIS difference spectra obtained on 308 nm photolysis of Orange II + photoinitiator in aqueous solution under N $_2$ , along with kinetics recorded at 500 and 650 nm. The TRVIS spectra show transient absorption at ca. 330–410 nm, bleaching at ca. 410–550 nm, and weak transient absorption at ca. 640–680 nm. The bleaching and transient absorption both increased over ca. 10  $\mu$ s, as shown by the kinetics at 500 nm, and both signals were significantly (ca.  $\times 20$ ) larger than those observed from Orange II in the absence of photoinitiator; an initial transient-absorption spike observed in the kinetic trace at 500 nm may be attributed to the photoinitiator triplet state (see above).

The TRVIS difference spectrum observed during the initial few microseconds is comparable to that reported for the Orange II radical anion generated by pulse radiolysis,<sup>33</sup> and the rise of the bleaching signal at ca. 500 nm (Figure 5) may be attributed to the loss of Orange II due to its reduction by the 2-hydroxy-2-propyl radicals formed on cleavage of the photoinitiator. The transient absorption at ca. 650 nm grows in with the bleaching of the parent dye and decays over ca. 100  $\mu$ s, and it may be attributed to the formation and reaction of the Orange II radical anion. The transient absorption at ca. 340 nm also grows in on the microsecond time scale and it may arise in part from the dye radical anion, but it may also include a contribution from photoinitiator products observed to absorb in this region from steady-state photolysis studies (Figure 3a).

The TRVIS kinetics were recorded as a function of laser pump energy. The magnitude of the bleach at ca. 500 nm and the observed rate of its rise were found to increase with the pump energy, with both effects being attributable to an increase in the concentration of 2-hydroxy-2-propyl radicals available to react with Orange II. The magnitude and observed rate of the rise in transient absorption at 650 nm, attributed to the dye radical anion, also increased with pump energy and may be attributed to the same effect; the observed decay rate at 650 nm also increased, suggesting that the subsequent reaction of the dye radical anion is not a first-order process, in agreement with previous work on similar dyes.<sup>30,31</sup>

The TRVIS kinetics were also recorded as a function of the initial Orange II concentration. As the Orange II concentration was increased from  $1 \times 10^{-5}$  to  $5 \times 10^{-4}$  mol dm $^{-3}$ , the observed bleach at ca. 500 nm increased progressively in both its magnitude and rate. At even higher Orange II concentrations of  $>5 \times 10^{-4}$  mol dm $^{-3}$ , the magnitude of the bleach became

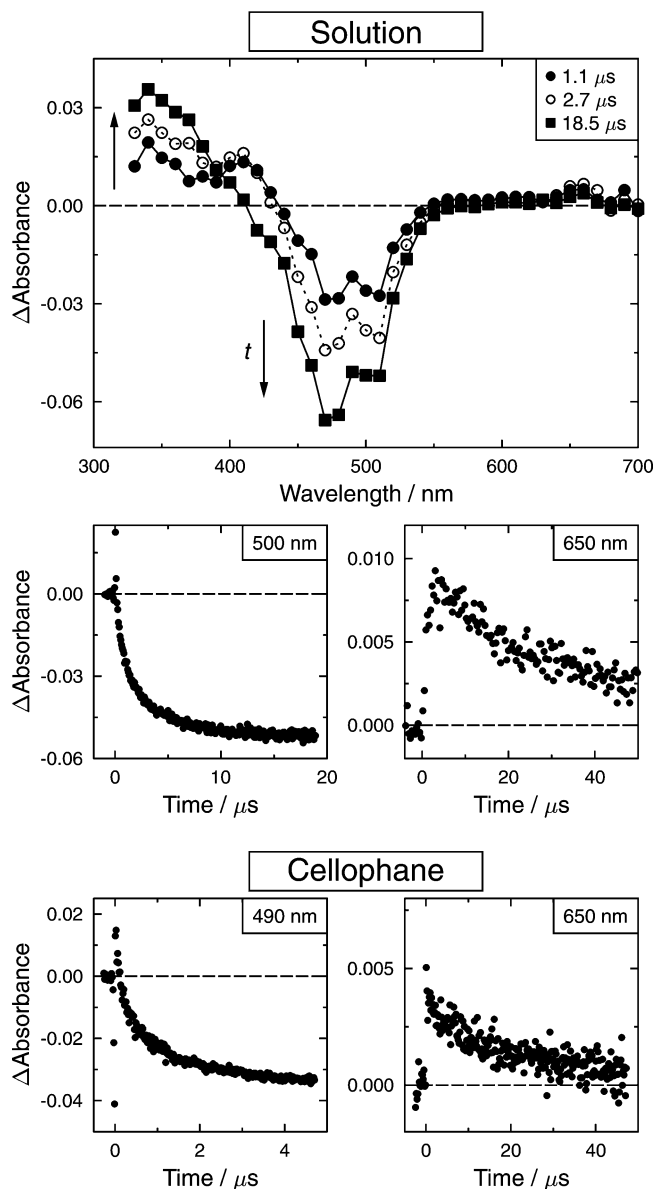
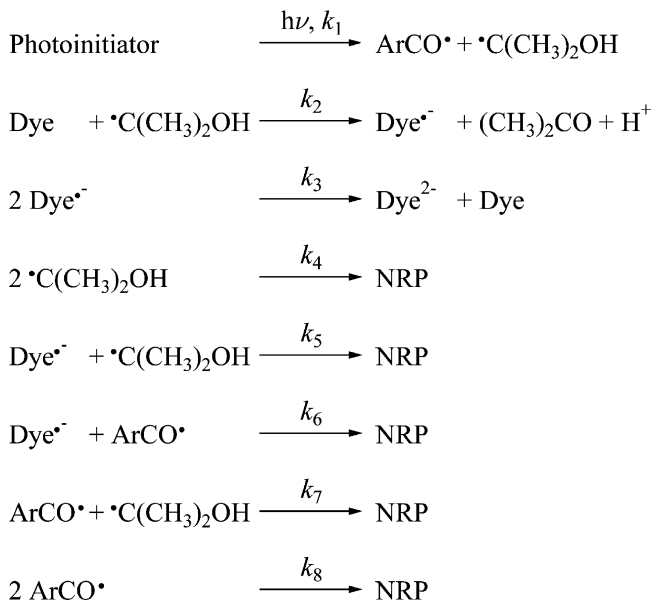


**Figure 5.** TRVIS difference spectra and kinetics of Orange II and photoinitiator: (top) in aqueous solution under  $N_2$  (at  $1 \times 10^{-4}$  and  $1 \times 10^{-3} \text{ mol dm}^{-3}$ , respectively); (bottom) in cellophane (at  $1.3 \times 10^{-2}$  and  $6.0 \times 10^{-2} \text{ mol dm}^{-3}$ , respectively).

progressively smaller but the initial rate of the bleaching was relatively unchanged. These trends may be understood as follows: as the dye concentration is increased, the reaction between Orange II and the 2-hydroxy-2-propyl radicals competes increasingly with other radical reactions, giving rise to a stronger bleach; the observed rate for this second-order process also increases. However, Orange II absorbs appreciably at the laser wavelength ( $\epsilon_{308} \approx 9600 \text{ dm}^3 \text{ mol}^{-1} \text{ cm}^{-1}$ ), giving rise to a screening effect as its concentration increases and it absorbs an increasing proportion of the pump photons, such that the extent of photoinitiator photolysis decreases significantly to give a lower concentration of photoinitiator radicals and a smaller bleaching signal. A quantitative treatment of self-absorption effects is included in the following section, which provides a detailed kinetic analysis.

**Detailed Kinetic Analysis.** Scheme 2 may be used generally to describe the photolysis of the photoinitiator, the subsequent reduction of a dye by 2-hydroxy-2-propyl radicals, the decay of dye radical anions by disproportionation to give the original

### SCHEME 2: General Mechanism for Dye Reduction Using Photoinitiator under $N_2$



dye and a hydrazine, and several possible side reactions of the dye radicals and other radicals; NRP indicates nonradical products that are assumed not to undergo any further reactions involving the species within Scheme 2 at least on the time scale of the kinetics being analyzed. It has been reported<sup>28</sup> that the rate constant for reaction between the benzoyl radicals from the photoinitiator,  $\text{ArCO}\cdot$ , and a range of other dyes is significantly smaller than that for reaction between the 2-hydroxy-2-propyl radicals and dyes (step 2), and so this reaction has not been included in Scheme 2. A full list of the corresponding rate equations for all the species in Scheme 2 is given in the Appendix.

The first stage of the kinetic analysis was to estimate a value for  $k_2$ , the rate constant for reduction of Orange II by 2-hydroxy-2-propyl radicals to form Orange II $^{\cdot-}$ . A consideration of the rate equations shows that the dye may show pseudo-first-order bleaching kinetics under some experimental conditions with appropriate concentrations of the various species (see Appendix), and this approach has been used to obtain reported rate constants for the reduction of various dyes by 2-hydroxy-2-propyl and similar radicals in pulse radiolysis and TRVIS studies.<sup>27–29</sup> Under the conditions used here, the bleaching kinetics were found to fit well to a single exponential rise only during the initial ca. 2–3  $\mu\text{s}$  after photolysis, showing significant deviations at later times that indicate pseudo-first-order kinetics do not fully apply and that such an analysis would not be rigorous for these data.<sup>41</sup> Nevertheless, this approach was used here to provide an initial estimate of  $k_2$ : the bleaching kinetics at 490 nm were fitted to single exponentials over the initial 3  $\mu\text{s}$ , and the corresponding rate constants were plotted versus the initial dye concentration,  $[\text{Orange II}]_0$ , to give a gradient that estimated  $k_2 = (4.3 \pm 0.8) \times 10^9 \text{ dm}^3 \text{ mol}^{-1} \text{ s}^{-1}$ , as shown in Figure 6 (left). The bleaching signal at 490 nm may contain a contribution not only from Orange II but also from other species, making further analysis nontrivial. In contrast, the transient absorption at 650 nm may be attributed solely to the Orange II radical anion and so this wavelength was used for the next stage of the analysis; neither Orange II (Figure 2a) nor the photoinitiator radicals  $\cdot\text{C}(\text{CH}_3)_2\text{OH}$  and  $\text{ArCO}\cdot$  (Figure 4) absorb appreciably at 650 nm, and the Orange II hydrazine is not expected to absorb strongly in the visible region. The transient absorption at 650

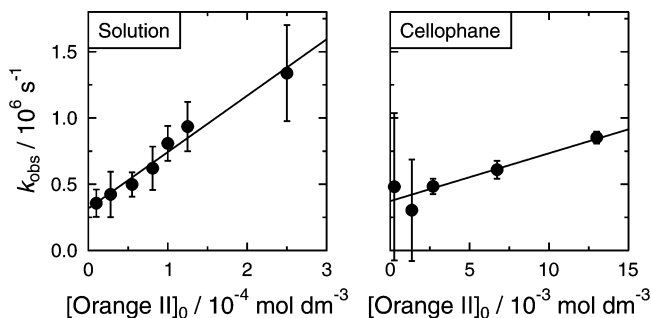


**Figure 6.** Linear fits of  $k_{\text{obs}}$  obtained from single-exponential fits of bleaching kinetics at 490 nm from Orange II + photoinitiator samples (error bars are  $\pm 2\sigma$  from the exponential fits), versus the initial Orange II concentration,  $[\text{Orange II}]_0$ , to obtain estimates for  $k_2$  in aqueous solution (left) and cellophane (right).

nm rises within ca. 5  $\mu\text{s}$  and decays in ca. 100  $\mu\text{s}$ , giving the time scale over which the Orange II radical anion is present.

A full analysis of the kinetics at 650 nm was performed using the eight-step mechanism in Scheme 2 as the kinetic model: the time-dependent concentration of each species was calculated by numerical integration of the corresponding rate equations and converted to absorbance using the Beer–Lambert Law. The first stage of the full analysis involved fitting four variable parameters, namely  $[\text{C}(\text{CH}_3)_2\text{OH}]_0$ ,  $k_2$ ,  $k_3$ , and  $\epsilon_{650}(\text{Dye}^{\bullet-})$ , to the kinetics recorded at eight different laser pump energies. An initial estimate of  $[\text{C}(\text{CH}_3)_2\text{OH}]_0 = 2 \times 10^{-4} \text{ mol dm}^{-3}$  was obtained<sup>42</sup> from the laser pump energy, beam size, photoinitiator absorbance, and reported dissociation quantum yield;<sup>36</sup> an initial estimate of  $k_2 = 4 \times 10^9 \text{ dm}^3 \text{ mol}^{-1} \text{ s}^{-1}$  came from the linear fit in Figure 6; an initial estimate of  $k_3 = 5 \times 10^8 \text{ dm}^3 \text{ mol}^{-1} \text{ s}^{-1}$  was based on literature values for comparable reactions;<sup>43</sup> and an initial estimate of  $\epsilon_{650}(\text{Dye}^{\bullet-}) = 3000 \text{ dm}^3 \text{ mol}^{-1} \text{ cm}^{-1}$  was used from a reported spectrum of the Orange II radical anion.<sup>27</sup> The other parameters in the kinetic model were fixed at this stage of the analysis: a literature value of  $k_4 = 6.5 \times 10^8 \text{ dm}^3 \text{ mol}^{-1} \text{ s}^{-1}$  was used for the self-termination of  $[\text{C}(\text{CH}_3)_2\text{OH}]$  in aqueous solution;<sup>44</sup> a literature value for the self-termination reaction of  $[\text{PhCO}^{\bullet}]$  in 3-methyl-3-pentanol<sup>45</sup> was used for  $k_8 = 5 \times 10^8 \text{ dm}^3 \text{ mol}^{-1} \text{ s}^{-1}$ ; and  $k_5$ ,  $k_6$ , and  $k_7$  were set to  $5 \times 10^8 \text{ dm}^3 \text{ mol}^{-1} \text{ s}^{-1}$  based on literature values for similar radical reactions in aqueous solution.<sup>43,46</sup> A total least-squares value from the full set of eight kinetic traces at 650 nm was used to determine the goodness of fit. A step-fit algorithm was used to explore a wide range of values for  $[\text{C}(\text{CH}_3)_2\text{OH}]_0$ ,  $k_2$ ,  $k_3$  and  $\epsilon_{650}(\text{Dye}^{\bullet-})$  to locate the region of the error surface corresponding to the global best fit,<sup>47</sup> and then a simplex algorithm was used to refine the fit, achieving a good overall fit to all of the kinetics recorded at 650 nm.

The second stage of the full analysis involved extending the fit to include the kinetics at 490 nm. The Orange II radical anion is reported to react by disproportionation<sup>30,31</sup> to form the hydrazine and regenerate the parent dye (step 3 in Scheme 2). A kinetic trace recorded in a region where only Orange II absorbs would therefore be expected to show some bleach recovery over ca. 100  $\mu\text{s}$ , on the same time scale as the decay of the radical anion absorption at 650 nm (Figure 5). The observed bleach at ca. 450–550 nm did not show significant recovery over ca. 100  $\mu\text{s}$ , suggesting that the signal at 490 nm not only arose from bleaching of Orange II but also contained a contribution from an overlying transient absorption due to the Orange II radical anion, in agreement with pulse-radiolysis studies that showed it absorbs appreciably across the ca. 380–650 nm region.<sup>27</sup> Consequently, a full analysis of the

**TABLE 1: Optimized Values<sup>a</sup> for Orange II Parameters Modeled Using Scheme 2**

$k_2$	$2.23 \times 10^9$
$k_3$	$2.61 \times 10^8$
$k_4$	$6.50 \times 10^8$ <sup>b</sup>
$k_5$	$2.33 \times 10^8$
$k_6$	$3.18 \times 10^8$
$k_7$	$1.74 \times 10^8$
$k_8$	$5.00 \times 10^8$ <sup>c</sup>
$\epsilon_{650}(\text{Dye}^{\bullet-})$	1340
$\epsilon_{490}(\text{Dye}^{\bullet-})$	8080
$[\text{C}(\text{CH}_3)_2\text{OH}]_0$	$2.4 \times 10^{-4}$ <sup>d</sup>

<sup>a</sup>  $k$  in  $\text{dm}^3 \text{ mol}^{-1} \text{ s}^{-1}$ ,  $\epsilon$  in  $\text{dm}^3 \text{ mol}^{-1} \text{ cm}^{-1}$ , and concentration in  $\text{mol dm}^{-3}$ . <sup>b</sup> Reference 44. <sup>c</sup> Reference 45. <sup>d</sup> Optimized value at the highest laser pulse energy, and scaled for lower pulse energies and some data sets as described in the text.

kinetics at 490 nm was obtained by fitting four variable parameters, namely  $[\text{C}(\text{CH}_3)_2\text{OH}]_0$ ,  $k_2$ ,  $k_3$ , and  $\epsilon_{490}(\text{Dye}^{\bullet-})$ , to the kinetics recorded at eight different laser pump energies, in parallel with maintaining a good fit to the kinetics at 650 nm with the same parameters, but using  $\epsilon_{650}(\text{Dye}^{\bullet-})$  rather than  $\epsilon_{490}(\text{Dye}^{\bullet-})$ , and with the fitted  $\Delta A$  at 490 nm obtained by subtracting the contribution of Orange II from that of its radical anion. The refined values from the fit to the data at 650 nm were used as initial estimates, along with the fixed values used in that fit, the fixed value of  $\epsilon_{490}(\text{Dye}^{\bullet-}) = 2 \times 10^4 \text{ dm}^3 \text{ mol}^{-1} \text{ cm}^{-1}$  measured here, and an estimated value of  $\epsilon_{490}(\text{Dye}^{\bullet-}) = 7000 \text{ dm}^3 \text{ mol}^{-1} \text{ cm}^{-1}$  from the literature<sup>27</sup> that was allowed to vary. A simplex algorithm was used to refine the fit of these five parameters to sixteen kinetic traces in parallel, i.e., the kinetics at 490 and 650 nm obtained at eight different laser pulse energies.

The third and final stage of the full analysis involved a simplex algorithm fit where all of the unknown parameters including  $k_{5-7}$  were allowed to vary to give the final set of optimized values listed in Table 1, which includes the best fits to all of the rate constants in Scheme 2 along with the best-fit values of  $\epsilon_{490}(\text{Dye}^{\bullet-})$ ,  $\epsilon_{650}(\text{Dye}^{\bullet-})$ , and  $[\text{C}(\text{CH}_3)_2\text{OH}]_0$  at the highest laser pulse energy, all of which were similar to the initial estimates. Selected kinetics recorded at 650 and 490 nm for several different laser energies are shown in Figure 7 (upper two sets), overlaid with modeled kinetics calculated from the optimized parameters in Table 1; further kinetics are shown in Figures S1 and S2 in the Supporting Information.

The optimized parameters in Table 1 were tested further by comparing the calculated kinetics with the observed bleach kinetics at 490 nm from five lower initial Orange II concentrations. The concentration dependence was incorporated into the modeling in two ways, first as the value of  $[\text{Orange II}]_0$  and second to give a scaled value of  $[\text{C}(\text{CH}_3)_2\text{OH}]_0$  arising from Orange II absorption at the laser wavelength reducing the proportion of incident photons available for photoinitiator photolysis (as described in Appendix SA1 in the Supporting Information). Selected kinetics recorded at 490 nm from three initial Orange II concentrations are shown in Figure 7 (lower set), overlaid with modeled kinetics calculated from the optimized parameters in Table 1, showing good fits to the data and providing additional support for the kinetic scheme and the fitted parameters;<sup>48</sup> further kinetics are shown in Figure S3 in the Supporting Information.

In summary, our full analysis gave a good fit to experimental data recorded under a wide range of conditions using the kinetic model in Scheme 2 and the parameters in Table 1. The modeled kinetics depended strongly on the values of  $k_2$  and  $k_3$ , giving

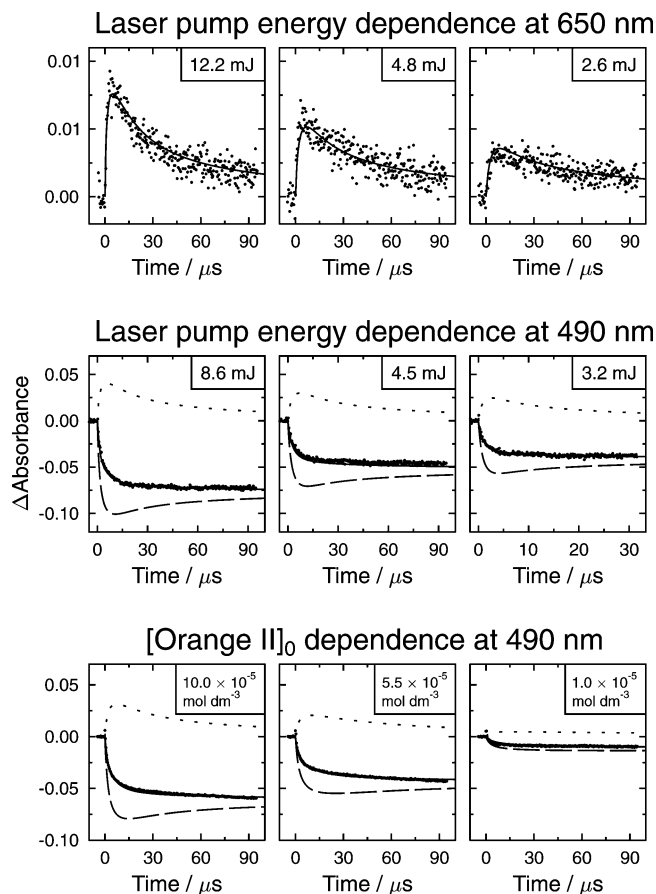


**Figure 7.** TRVIS kinetics of Orange II and photoinitiator in aqueous solution (•) overlaid with kinetics modeled using the parameters in Table 1. Laser pump energy dependence: Orange II and photoinitiator at  $1 \times 10^{-4}$  and  $1 \times 10^{-3}$  mol dm $^{-3}$ , respectively, recorded at 650 nm (top; average of 32 laser pulses) and 490 nm (middle; average of 16 laser pulses). Initial Orange II concentration dependence: photoinitiator at  $1 \times 10^{-3}$  mol dm $^{-3}$ , and recorded at 490 nm (bottom; average of 32 laser pulses). The modeled overall contribution at 490 nm (solid line) is shown along with individual calculated contributions from Orange II (dashed line) and Orange II $^{\cdot-}$  (dotted line).

good confidence in their fitted values, whereas the other rate constants showed a weaker dependence. The value of  $k_2 = 2.2 \times 10^9$  dm $^3$  mol $^{-1}$  s $^{-1}$  obtained here is similar to that of  $2.7 \times 10^9$  dm $^3$  mol $^{-1}$  s $^{-1}$  reported for the same reaction determined from a pseudo-first-order fit to pulse radiolysis data.<sup>27</sup> The absorption coefficients of 8080 and 1340 dm $^3$  mol $^{-1}$  cm $^{-1}$  at 490 and 650 nm, respectively, obtained here for the Orange II radical anion are comparable to those of ca. 8100 and 3700 dm $^3$  mol $^{-1}$  cm $^{-1}$  reported previously,<sup>27</sup> within the uncertainties of these measurements, and to those of ca. 9500 and 500 dm $^3$  mol $^{-1}$  cm $^{-1}$  reported for the Acid Orange 12 radical anion (a structural isomer of Orange II with a sulfonated naphthyl rather than phenyl ring).<sup>31</sup>

The kinetic model enables the concentration of each species to be estimated at all times. If it is assumed that only Orange II and its radical anion absorb appreciably in the visible region, then the spectrum of the radical anion can be estimated, as shown in Figure 8 where the Orange II spectrum scaled to its estimated concentration at 18.5  $\mu$ s has been added to the observed TRVIS spectrum at that time (Figure 5). The estimated radical anion spectrum shows bands at ca. 400 and 500 nm, and a much weaker feature at ca. 650 nm, and within the uncertainties of these measurements it is comparable to that reported for the radical anions of Orange II<sup>27</sup> and Acid Orange 12<sup>31</sup> measured after pulse radiolysis.

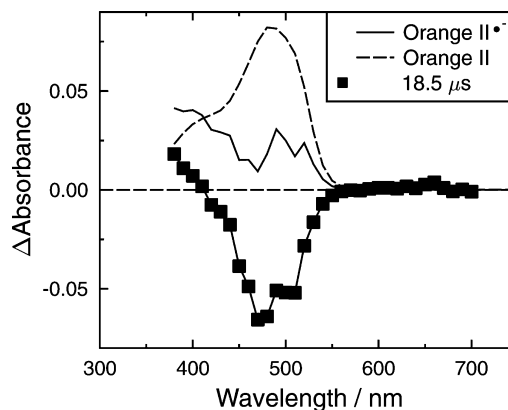


**Figure 8.** Orange II radical anion spectrum in aqueous solution (solid line) estimated by adding the Orange II spectrum (dashed line), scaled to its calculated concentration at 18.5  $\mu$ s, to the experimental TRVIS spectrum recorded at this time (Figure 5).

A TRVIS difference spectrum recorded 3 ms after photolysis, given in Figure 3b, shows that the transient absorption at ca. 650 nm assigned solely to the radical anion had decayed, whereas both the transient absorption at  $<400$  nm and the main bleach band of Orange II band at ca. 490 nm were still present with magnitudes similar to those observed in the TRVIS difference spectra at ca. 20  $\mu$ s (Figure 5). However, the TRVIS spectrum at 3 ms was not identical to the difference spectrum from the steady-state photolysis study, with which it is overlaid in Figure 3b for comparison; a bleaching shoulder at ca. 410 nm that mirrors the shoulder in the spectrum of Orange II (Figure 2a) is present in the TRVIS spectrum at 3 ms but absent in the steady-state difference spectrum (Figure 3b), and transient absorption at  $<390$  nm that is clearly present at 3 ms is weaker in the steady-state difference spectrum. Together, these observations suggest that the new species giving a distinct absorption band at 413 nm in the steady-state photolysis experiments (Figure 2c) forms at  $>3$  ms, and that its formation is accompanied by the loss of a species that absorbs at ca.  $<390$  nm.

**Steady-State Photolysis Studies in Cellophane.** Figure 9 shows steady-state UV–visible absorption spectra recorded during photolysis of cellophane samples containing (a) Orange II alone and (b) Orange II + photoinitiator. The sample of Orange II alone showed negligible ( $<1\%$ ) fading after 12 flashgun pulses. The sample with added photoinitiator showed a ca. 10% decrease in the photoinitiator band at ca. 270 nm, attributable to photoinitiator photolysis, and a ca. 2% decrease in the main absorption band of Orange II after 12 pulses that is attributable to its reduction by 2-hydroxy-2-propyl radicals and that is smaller than the ca. 17% decrease shown by a comparable solution sample after a single pulse (Figure 2c).

**TRVIS Studies of Photoinitiator Alone in Cellophane.** The TRVIS spectra recorded on photolysis of the photoinitiator alone in wet cellophane, shown in Figure 4, are similar to those from aqueous solution, as also shown in Figure 4, and they may be assigned similarly to the triplet state. However, the kinetics from the two samples are different; the fast decay of  $\tau = 113 \pm 20$  ns observed from the solution sample was observed also from the cellophane sample but there was an additional, slower component, such that the data fitted well to a biexponential decay with lifetimes of  $\tau_1 = 112 \pm 7$  ns and  $\tau_2 = 1.30 \pm 0.06$   $\mu$ s (Figure 4); the relative magnitudes of the two components did not change significantly across the wavelength range studied, suggesting two parallel decay routes. The observation of two lifetimes for the photoinitiator triplet state suggests that it may

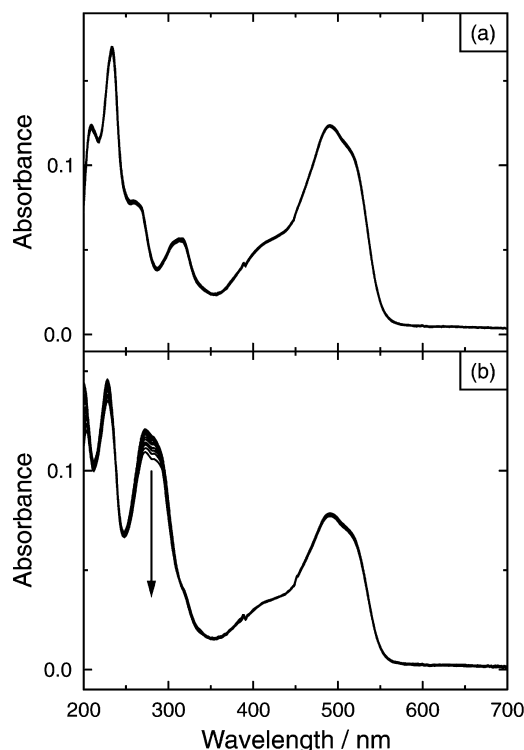


**Figure 9.** Steady-state UV-visible absorption spectra of (a) Orange II at  $1.3 \times 10^{-3} \text{ mol dm}^{-3}$  and (b) Orange II and photoinitiator at  $0.9 \times 10^{-4}$  and  $1.1 \times 10^{-3} \text{ mol dm}^{-3}$ , respectively, in cellophane recorded during photolysis with a camera flashgun (12 pulses each).

be present in two distinct environments within the cellophane, with one environment comparable to that in solution; this interpretation is consistent with EPR studies that showed two sets of signals from the photoinitiator alone in cotton, with one set comparable to that in solution and attributed to radicals in liquid-like amorphous regions of cellulose, and another set attributed to the same radicals adsorbed on the surfaces of crystallites.<sup>49</sup>

**TRVIS Studies of Orange II Alone in Cellophane.** TRVIS studies of Orange II alone in cellophane gave weak bleaching and transient absorption signals at 490 and 410 nm, respectively, which rose with the instrument-response time and showed little or no decay over  $20 \mu\text{s}$ , and which were much smaller than those observed from Orange II in the presence of photoinitiator in cellophane discussed below; both dry and wet cellophane samples gave similar results, which are comparable to those from Orange II alone in solution, as discussed above. UV-visible spectra recorded before and after the TRVIS experiments showed negligible ( $\ll 1\%$ ) change.

**TRVIS Studies of Orange II + Photoinitiator in Cellophane.** Initial studies of cellophane samples that had been dried after soaking in the mixed Orange II + photoinitiator solution showed only very small TRVIS signals. In contrast, cellophane samples that were kept wet gave larger signals that were suitable for further study, although the signals were smaller than those from comparable solution samples excited by similar laser pump energies.

The TRVIS data from wet cellophane samples were found to be similar to those from solution samples of Orange II + photoinitiator, as shown by the kinetic traces in Figure 5, and they may be attributed to the same processes. However, kinetics that are observed to be similar may arise from second-order rate constants that are significantly lower in cellophane than in solution, as discussed further below, because of the higher

concentrations used to give similar absorbances from the cellophane and solution samples with path lengths of ca.  $45 \mu\text{m}$  and  $1 \text{ mm}$ , respectively. The kinetics recorded at  $490 \text{ nm}$  from a wet cellophane sample showed a short-lived transient absorption attributable to the photoinitiator triplet state at early times, and a bleaching rise over ca.  $4 \mu\text{s}$  attributable to loss of Orange II on reduction by 2-hydroxy-2-propyl radicals; those recorded at  $650 \text{ nm}$  showed transient absorption that rose over several microseconds and decayed over ca.  $50 \mu\text{s}$ , attributable to the Orange II radical anion.

The kinetics at  $490 \text{ nm}$  were recorded as a function of the initial dye concentration in cellophane. As the Orange II concentration was increased from  $3 \times 10^{-3}$  to  $13 \times 10^{-3} \text{ mol dm}^{-3}$ , the observed bleach increased progressively in both its magnitude and rate, showing behavior that was similar to that observed from solution samples; it may be attributed similarly to Orange II competing increasingly effectively for the 2-hydroxy-2-propyl radicals to give a stronger bleach with an increased rate. As the Orange II concentration was decreased from  $3.0 \times 10^{-3}$  to  $0.3 \times 10^{-3} \text{ mol dm}^{-3}$ , the bleach decreased in magnitude such that the signal at  $490 \text{ nm}$  became a weak transient absorption that was similar to that observed from photoinitiator alone in cellophane (Figure 4) due to a lower yield of dye reduction.

The requirement to translate the cellophane samples between each laser shot precluded the recording of TRVIS spectra and kinetics across the wide range of conditions needed for a detailed kinetic-modeling analysis. The bleaching kinetics at  $490 \text{ nm}$  from the cellophane samples at  $[\text{Orange II}]_0 = (3\text{--}13) \times 10^{-3} \text{ mol dm}^{-3}$  were found to fit well to a single exponential rise during  $0\text{--}5 \mu\text{s}$ , consistent with pseudo-first-order bleaching kinetics being more valid for the cellophane samples than for the solution samples at lower dye concentrations, as discussed above; however, the signal may also contain overlying transient absorption contributions from the dye radical anion and the long-lived photoinitiator triplet state in cellophane. A plot of the observed rate constants versus the initial dye concentration shown in Figure 6 gave a gradient that estimated  $k_2(\text{cellophane}) \approx (3.6 \pm 2.7) \times 10^7 \text{ dm}^3 \text{ mol}^{-1} \text{ s}^{-1}$ , which is approximately two orders of magnitude lower than the solution value of  $k_2 = 2.2 \times 10^9 \text{ dm}^3 \text{ mol}^{-1} \text{ s}^{-1}$  (Table 1) obtained from the full kinetic analysis (and  $k_2 \approx 4.3 \times 10^9 \text{ dm}^3 \text{ mol}^{-1} \text{ s}^{-1}$  estimated by the same linear analysis that is also shown in Figure 6). The rate constant for azo dye reduction by photoinitiator radicals has been reported to be lower in cotton than in solution,<sup>29</sup> and it was proposed to result from a lower rate constant for diffusion in cellophane because EPR studies have shown that some radicals in cotton behave as if they are in a liquid environment with a viscosity of ca.  $20\text{--}30 \text{ cP}$ <sup>49–51</sup> that is much higher than that of ca.  $1 \text{ cP}$  for water.<sup>52</sup> A similar effect may apply here because of the structural similarity of cellophane and cotton, both being porous forms of cellulose.

**HPLC Product Studies.** Reverse-phase HPLC was used to identify the products from the electrochemical and steady-state photolysis studies by making comparisons with the retention times ( $RT$ ), and the UV-visible spectra and absorption maxima ( $\lambda_{\text{max}}$ ) of a range of known samples used as standards; peak integrations were used to estimate concentrations. The spectra of major products and relevant standards are shown in Figure S4 in the Supporting Information.

**Orange II Alone.** Under the HPLC conditions used here, Orange II eluted at ca.  $21.8 \text{ min}$ . Figure 10a gives the chromatogram from a sample extracted after electrochemical reduction of Orange II at  $5.0 \times 10^{-4} \text{ mol dm}^{-3}$ , showing residual

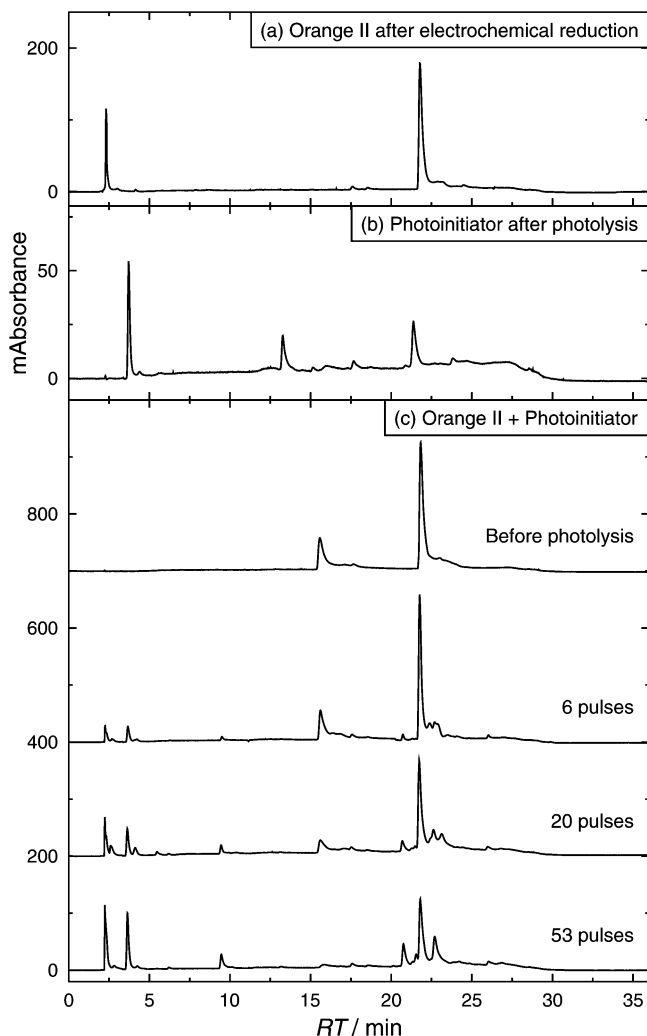
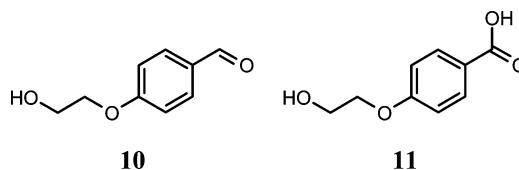


**Figure 10.** HPLC chromatograms recorded at 254 nm of (a) Orange II after electrochemical reduction ( $5 \times 10^{-4}$  mol  $\text{dm}^{-3}$ ), (b) photoinitiator after photolysis under  $\text{N}_2$  ( $5 \times 10^{-4}$  mol  $\text{dm}^{-3}$ ), (c) Orange II + photoinitiator before and after photolysis with a camera flashgun under  $\text{N}_2$  (both at  $5 \times 10^{-4}$  mol  $\text{dm}^{-3}$ ). Spectra of the major components are given in Figure S4 in the Supporting Information.

Orange II at  $2.3 \times 10^{-4}$  mol  $\text{dm}^{-3}$  (ca. 46% of its initial concentration) and a strong new peak with  $RT \approx 2.5$  min and a spectrum ( $\lambda_{\text{max}} = 249, 283\text{sh}$  nm) that matches that from a known sample of 4-aminobenzenesulfonic acid, and for which the concentration was estimated as  $1.6 \times 10^{-4}$  mol  $\text{dm}^{-3}$  (ca. 32% of the initial dye concentration). The observation of 4-aminobenzenesulfonate is consistent with reduction leading to cleavage of the N–N bond; several other minor, unidentified peaks were also observed but none of these could be assigned confidently to products arising from the naphthyl moiety of the dye.

**Photoinitiator Alone.** The photoinitiator alone eluted at ca. 15.6 min. Figure 10b gives the chromatogram from a sample extracted after photolysis of the photoinitiator at  $5 \times 10^{-4}$  mol  $\text{dm}^{-3}$  under  $\text{N}_2$ , showing residual photoinitiator at ca. 2% of its initial concentration and three strong new peaks at ca. 3.7 min ( $\lambda_{\text{max}} = 247$  nm), 13.3 min ( $\lambda_{\text{max}} = 283$  nm), and 21.4 min ( $\lambda_{\text{max}} = 299$  nm) that will contribute to the positive features observed in the difference spectrum obtained on steady-state photolysis (Figure 3a). Products formed solely from the 2-hydroxy-2-propyl moiety are unlikely to absorb appreciably in the UV–visible region, and so the photoinitiator products detected are attributed to the substituted benzoyl moiety (Scheme 1), for which one

possible reaction is hydrogen abstraction to give a substituted benzaldehyde. Samples of unsubstituted benzaldehyde and unsubstituted benzoic acid eluted with  $RT \approx 19.9$  and 4.6 min, respectively, and the photoinitiator products that eluted at ca. 21.4 and 3.5 min are identified as the substituted benzaldehyde **10** and benzoic acid **11** (shown below), at concentrations of ca.  $1.7 \times 10^{-4}$  and  $1.5 \times 10^{-4}$  mol  $\text{dm}^{-3}$  estimated by assuming that their peak absorption coefficients are the same as those of the unsubstituted analogues; the shorter retention times indicate that benzoic acid and **11** are present as benzoates in the HPLC mobile phase at pH 5.2, consistent with a  $\text{p}K_{\text{a}}$  of 4.2 for benzoic acid.<sup>52</sup> The route for formation of **11** is unclear, but its presence may be attributed to reaction of the substituted benzoyl radical (e.g., with trace amounts of  $\text{O}_2$ , the photoinitiator, or another species). The relative abundance of products **10** and **11** was not studied in detail but was found to depend on the photolysis conditions, including the initial photoinitiator concentration, the method of photolysis (i.e., flashgun or continuous lamp irradiation), and whether the sample was under  $\text{N}_2$  or air (the relative abundance of **11** was higher under air).



The product eluting at 13.3 min ( $\lambda_{\text{max}} = 283$  nm) was not identified but its absorption spectrum suggests that it also is a substituted aromatic species, and in contrast to **10** and **11**, it was not observed on photolysis of the photoinitiator in the presence of Orange II (see below), suggesting that the route for its formation may involve 2-hydroxy-2-propyl radicals that react predominantly with the dye when Orange II is present. Several other unidentified species were observed as weak peaks, consistent with the presence of several cross-products.

**Orange II + Photoinitiator.** HPLC chromatograms from samples extracted before and during photolysis of an equimolar Orange II + photoinitiator sample ( $5 \times 10^{-4}$  mol  $\text{dm}^{-3}$ ) under  $\text{N}_2$  are given in Figure 10c. The strong peaks arising from Orange II ( $RT \approx 21.8$  min) and photoinitiator ( $RT \approx 15.6$  min) decreased progressively with the extent of photolysis; after 53 flashgun pulses, the photoinitiator could no longer be detected but residual Orange II was present at ca.  $1.5 \times 10^{-4}$  mol  $\text{dm}^{-3}$  (ca. 30% of its initial concentration). The photoinitiator products **10** ( $RT \approx 21.3$  min) and **11** ( $RT \approx 3.6$  min) grew in with the extent of photolysis; the concentration of **10** could not be estimated because its peak overlapped with a much stronger peak of Orange II, but the concentration of **11** was estimated as ca.  $2.7 \times 10^{-4}$  mol  $\text{dm}^{-3}$  from a distinct peak. The photoinitiator product eluting at ca. 13.3 min was not observed from this sample, as discussed above.

Several other species grew in with the extent of photolysis, and spectra of the main features are shown in Figure S4 in the Supporting Information. A species with  $RT \approx 2.2$  min ( $\lambda_{\text{max}} = 249, 283\text{sh}$  nm) is assigned to 4-aminobenzenesulfonate at an estimated concentration of ca.  $1.6 \times 10^{-4}$  mol  $\text{dm}^{-3}$  (Figure S4). An unidentified species with  $RT \approx 22.6$  min ( $\lambda_{\text{max}} = 486, 255, 230$  nm) had a similar retention time and UV–visible spectrum to that of Orange II ( $RT \approx 21.8$  min;  $\lambda_{\text{max}} = 484, 310, 255$  nm), giving a relatively weak visible band that will contribute little to the spectrum obtained on steady-state photolysis (Figure 2c) and stronger absorption at  $<350$  nm

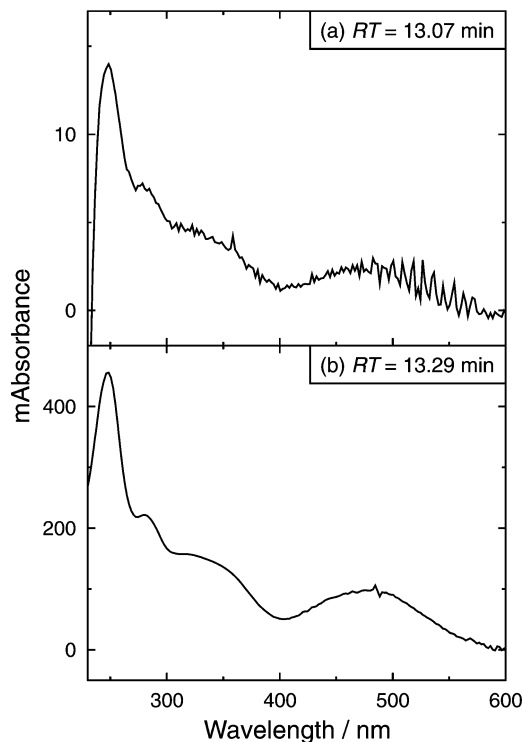


**Figure 11.** UV–visible spectra of species with  $RT \approx 13$  min from HPLC analysis of (a) 1:10 Orange II:photoinitiator after photolysis and subsequent bubbling with air and (b) product formed by reacting 1,2-naphthoquinone with 4-aminobenzenesulfonic acid.

(Figure S4), and it may arise from the addition of a radical species to Orange II. Another species with  $RT \approx 20.7$  min ( $\lambda_{\max} = 412, 278$  nm) gave a strong visible absorption band (Figure S4) that matched the band at 413 nm that became prominent on photolysis under  $N_2$  (Figure 2c). Further unidentified species were observed, including a strong peak at  $RT \approx 9.5$  min ( $\lambda_{\max} = 279$  nm) and several weaker peaks.

A further HPLC study was performed on a sample of Orange II + photoinitiator that had been photolyzed under  $N_2$  and then exposed to air. The species with  $RT \approx 20.7$  min ( $\lambda_{\max} = 412, 278$  nm) observed following photolysis under  $N_2$  (see above) was absent but a new species with  $RT \approx 13.1$  min and a visible band ( $\lambda_{\max} \approx 480$  nm), shown in Figure 11a, was observed that was not observed from samples kept under  $N_2$ . The absorption maximum of this species is similar to that of Orange II, but the overall spectra were a poor match and the unidentified species eluted ca. 7 min earlier. These observations are consistent with the steady-state photolysis study of Orange II + photoinitiator under  $N_2$ , where a strong band at ca. 413 nm became prominent on photolysis (Figure 2c) and was stable under  $N_2$ , but decreased on subsequent exposure to air as a strong new band at ca. 500 nm appeared (Figure 2d).

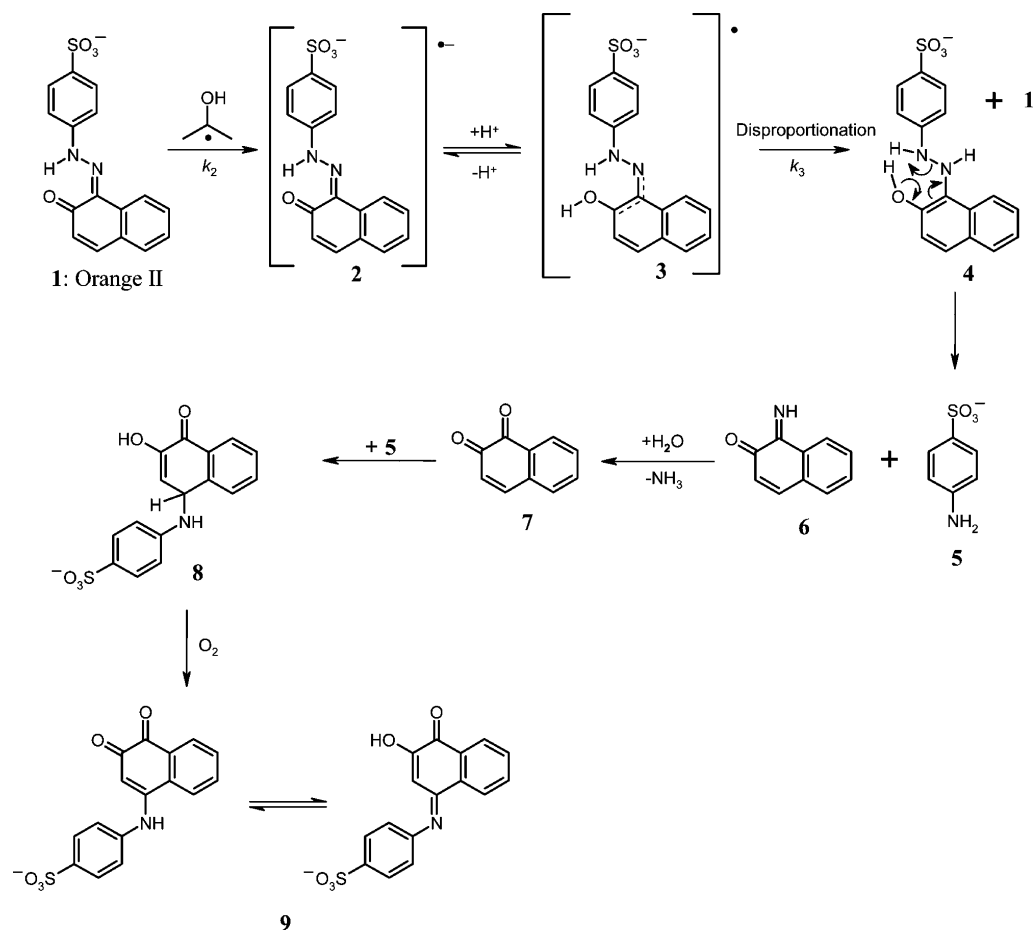
As with the analysis of the electrochemically reduced sample, none of the observed species could be identified conclusively as arising from the naphthyl moiety of Orange II. Literature reports of degradation studies of Orange II and similar azo dyes have also discussed the absence of observable naphthyl-based products, attributing their absence to the susceptibility of naphthoquinones and aminonaphthols to hydrolysis, oxidation, and other reactions that occur rapidly in aqueous solution.<sup>13,17,53</sup> In the current study, test samples of 1,2-naphthoquinone, 1,2-naphthalenediol, and 1-amino-2-naphthol could not be identified conclusively by HPLC due to their limited solubility in water and decomposition in aqueous solution.

The Orange II concentration was decreased by ca.  $3.5 \times 10^{-4}$  mol  $dm^{-3}$  on photolysis of the Orange II + photoinitiator sample, and so the maximum concentration of the dye products was ca.  $3.5 \times 10^{-4}$  mol  $dm^{-3}$ . A phenyl fragment of the dye was detected in the form of 4-aminobenzenesulfonate at ca.  $1.6 \times 10^{-4}$  mol  $dm^{-3}$ , accounting for approximately half of the phenyl-based Orange II products. To test the possibility that 4-aminobenzenesulfonate had formed in higher yield but some had reacted with naphthyl-based products, 4-aminobenzenesulfonate was mixed with 1,2-naphthoquinone in aqueous solution under air; 1,2-naphthoquinone is sparingly soluble in water but after several hours of stirring, no solid remained and the solution had changed from pale yellow to a deep orange color. An HPLC analysis of this solution showed a species with  $RT \approx 13.1$  min ( $\lambda_{\max} \approx 480$  nm) that was a good match with that of the product observed in the Orange II + photoinitiator sample that had been photolyzed under  $N_2$  and then exposed to air, as shown by the spectra in Figure 11. Further tests showed that the same product was obtained on mixing 4-aminobenzenesulfonate with 1-amino-2-naphthol in aqueous solution under air; its formation can be attributed to oxidation and hydrolysis yielding 1,2-naphthoquinone, which then reacts with 4-aminobenzenesulfonate to give the same final product. Sodium 1,2-naphthoquinone-4-sulfonate has been used as a standard test for primary aromatic amines,<sup>54–57</sup> where the pale yellow quinone solution turns a deep red color due to indophenol dyes formed by nucleophilic substitution of the amine at the 4-position of the quinone. It has also been reported that some aromatic amines react readily with 1,2-naphthoquinone in methanol<sup>58</sup> to give indophenol dyes with absorption maxima in the range of ca. 450–520 nm, depending on the amine. Thus, it is likely that the species with  $RT \approx 13.1$  min ( $\lambda_{\max} \approx 480$  nm) observed after photochemical reduction of Orange II under  $N_2$  and subsequent exposure to air is an indophenol dye.

**Reductive Degradation Mechanisms.** Combining the results from the steady-state studies, the TRVIS studies, the kinetic modeling, and the HPLC product studies enables the photoinitiator-induced, one-electron reductive fading mechanism of Orange II (**1**) to be described in detail, as shown in Scheme 3. It is well established that 2-hydroxy-2-propyl radicals are efficient one-electron donors that readily reduce an azo dye to its radical anion (**2**).<sup>5,27–29</sup> The radical anions of substituted azobenzenes are reported to have  $pK_a$  values in the range of ca. 13–18 and to protonate rapidly to form hydrazyl radicals at neutral pH,<sup>59–61</sup> and the rapid protonation of azo dye radical anions at neutral pH is commonly inferred in the literature.<sup>31</sup> Orange I and its radical anion are reported to have  $pK_a$  values of 8.3 and 7.9, respectively;<sup>30</sup> it is a structural analogue of Orange II with a 4-hydroxynaphthyl rather than a 2-hydroxynaphthyl group. Orange II is reported<sup>62</sup> to have a  $pK_a$  of 10.7 that is higher than that of Orange I, attributable to intramolecular hydrogen bonding at the 2-hydroxynaphthyl group, and its radical anion is also likely to have a higher  $pK_a$  than that of Orange I; hence, it is likely to protonate rapidly to give the hydrazyl radical **3** at the neutral pH used in the present studies (as shown in Scheme 3), and as our earlier EPR studies<sup>32</sup> showed that it did at pH 4.

The full kinetic analysis shows that the Orange II radical anion, observed directly in the TRVIS studies, decays principally by disproportionation to regenerate the parent dye **1**, as also observed by TRVIS, and the hydrazine, **4**. The 2-hydroxyl group of **4** provides a route for its rapid decay to give 4-aminobenzenesulfonate **5**, which is observed here as a final product by HPLC, and the imine **6**,<sup>63</sup> which is not observed here but is

## SCHEME 3: One-Electron Reduction Mechanism of Orange II



reported to hydrolyze to 1,2-naphthoquinone, **7**, with a half-life that is ca. 200 s in 90:10 aqueous ethanol and shorter at lower ethanol ratios.<sup>64</sup> **7** is not observed here but its presence is strongly inferred because HPLC shows that the same indophenol dye **9** produced on simple mixing of **5** and **7** under air is present after exposing the photolyzed Orange II + photoinitiator sample to air. The indophenol dye **9** is observed by UV-visible spectra to be produced on admitting air to a precursor that is stable under N<sub>2</sub> and that we tentatively assign to **8**, which is produced by nucleophilic attack by **5** on **7**; this assignment is based on the reported mechanism for the attack of **5** on 1,2-naphthoquinone-4-sulfonate,<sup>56</sup> used to tests for aromatic amines. We attribute the relative stability of **8** under N<sub>2</sub> to the lack of a sulfonate leaving group, such that the presence of oxygen is required for its oxidation to **9**.

The electrochemical reduction of azo and hydrazone dyes has been shown generally to occur via a 4-electron process overall, with a 2-electron reduction of the dye to the corresponding hydrazine followed by a further 2-electron reduction of the hydrazine to yield two aromatic primary amines from scission of the N–N bond.<sup>65</sup> The observation of 4-aminobenzene-sulfonate **5** after electrochemical reduction of Orange II suggests that a similar electrochemical reduction process occurs in this case. The other expected product, 1-amino-2-naphthol, was found to have low solubility in water and was not detected here, although it seems likely to have been produced; the 1-amino-2-naphthoxy radical has been observed by EPR on electrochemical reduction of Orange II.<sup>39</sup>

## Conclusions

The one-electron reductive fading mechanism of the azo dye Orange II in solution has been studied from initial radicals to final products, using 2-hydroxy-2-propyl radicals from a photoinitiator to induce the reaction. Nanosecond time-resolved UV-visible studies have enabled both the formation of the dye radical anion and its subsequent disproportionation to a hydrazine species to be observed, and their rate constants determined by detailed kinetic modeling based on an eight-step scheme. Parallel studies using steady-state photolysis with UV-visible monitoring and HPLC analysis have enabled the final products to be identified by comparison with standard samples, the products of test reactions, or the literature. Together, this combination of approaches has provided a consistent set of results that has enabled a detailed one-electron reduction mechanism to be proposed for Orange II; the observation of a reductive fading mechanism that involves not only the expected loss of the original azo chromophore but also the production of a different indophenol chromophore from the fragments is notable.

Studies of Orange II in cellophane suggest that the initial steps of the one-electron reduction mechanism are similar to those in solution, although the rate constant for reduction is approximately two orders of magnitude lower. This information could assist in understanding azo dye reactions in other cellulose environments, such as those provided by paper and cotton, where reduction reactions may be important.

**Acknowledgment.** We thank J. Oakes for helpful discussions, and we acknowledge the support of Unilever Research.

## Appendix

**Full Kinetic Analysis.** The time-dependent concentrations of the main species of interest in Scheme 2 can be determined using the following set of differential rate equations, which were used for numerical integration in the full kinetic modeling analysis:

$$\frac{d[{}^{\bullet}\text{C}(\text{CH}_3)_2\text{OH}]}{dt} = k_1[\text{PI}] - k_2[{}^{\bullet}\text{C}(\text{CH}_3)_2\text{OH}][\text{Dye}] - 2k_4[{}^{\bullet}\text{C}(\text{CH}_3)_2\text{OH}]^2 - k_5[{}^{\bullet}\text{C}(\text{CH}_3)_2\text{OH}][\text{Dye}^{\bullet-}] - k_7[{}^{\bullet}\text{C}(\text{CH}_3)_2\text{OH}][\text{ArCO}^{\bullet}] \quad (\text{A1.1})$$

$$\frac{d[\text{Dye}]}{dt} = -k_2[{}^{\bullet}\text{C}(\text{CH}_3)_2\text{OH}][\text{Dye}] + k_3[\text{Dye}^{\bullet-}]^2 \quad (\text{A1.2})$$

$$\frac{d[\text{Dye}^{\bullet-}]}{dt} = k_2[{}^{\bullet}\text{C}(\text{CH}_3)_2\text{OH}][\text{Dye}] - 2k_3[\text{Dye}^{\bullet-}]^2 - k_5[{}^{\bullet}\text{C}(\text{CH}_3)_2\text{OH}][\text{Dye}^{\bullet-}] - k_6[\text{Dye}^{\bullet-}][\text{ArCO}^{\bullet}] \quad (\text{A1.3})$$

$$\frac{d[\text{Dye}^{2-}]}{dt} = k_3[\text{Dye}^{\bullet-}]^2 \quad (\text{A1.4})$$

$$\frac{d[\text{ArCO}^{\bullet}]}{dt} = k_1[\text{PI}] - k_6[\text{Dye}^{\bullet-}][\text{ArCO}^{\bullet}] - k_7[{}^{\bullet}\text{C}(\text{CH}_3)_2\text{OH}][\text{ArCO}^{\bullet}] - 2k_8[\text{ArCO}^{\bullet}]^2 \quad (\text{A1.5})$$

**Approximations for Pseudo-First-Order Analysis.** Inspection of eq A1.2 suggests that under conditions where  $[\text{Dye}]_0 \gg [{}^{\bullet}\text{C}(\text{CH}_3)_2\text{OH}]_0$ , the reduction of the dye (step 2 in Scheme 2) will be pseudo-first order; i.e.,  $[\text{Dye}]$  will decay exponentially, at least initially where  $[\text{Dye}^{\bullet-}]$  is zero or very low. At later times, depending on the value of  $k_3$  and  $[\text{Dye}^{\bullet-}]$ , the kinetics will diverge from exponential as the dye partially recovers by disproportionation of the dye radical anion (step 3 in Scheme 2). Where the pseudo-first-order conditions apply, bleaching kinetics recorded at a wavelength where the dye absorbs should fit well to an exponential rise, and a plot of  $k_{\text{obs}}$  vs  $[\text{Dye}]_0$  will give a gradient of  $k_2$ .

A pseudo-first order reaction between the dye and  ${}^{\bullet}\text{C}(\text{CH}_3)_2\text{OH}$  is also approximated by integrating a simplified form of eq A1.1 in which the  $k_1[\text{PI}]$  term is omitted because  ${}^{\bullet}\text{C}(\text{CH}_3)_2\text{OH}$  forms on a faster time scale than the subsequent processes in Scheme 2, and in which  $[\text{Dye}]$ ,  $[\text{Dye}^{\bullet-}]$ , and  $[\text{ArCO}^{\bullet}]$  are held constant, to give eq A1.6.

$$[{}^{\bullet}\text{C}(\text{CH}_3)_2\text{OH}]_t = \frac{k_{\text{obs}}[{}^{\bullet}\text{C}(\text{CH}_3)_2\text{OH}]_0 \exp(-k_{\text{obs}}t)}{k_{\text{obs}} + 2k_4[{}^{\bullet}\text{C}(\text{CH}_3)_2\text{OH}]_0 \{1 - \exp(-k_{\text{obs}}t)\}} \quad (\text{A1.6})$$

where

$$k_{\text{obs}} = k_2[\text{Dye}] + k_5[\text{Dye}^{\bullet-}] + k_7[\text{ArCO}^{\bullet}]$$

If  $[\text{Dye}]$  is in large excess to give  $k_{\text{obs}} \approx k_2[\text{Dye}]$ , then eq A1.6 simplifies to a single exponential decay of  $[{}^{\bullet}\text{C}(\text{CH}_3)_2\text{OH}]$ , eq A1.7, that matches the single exponential dye bleaching kinetics approximated above.

$$[{}^{\bullet}\text{C}(\text{CH}_3)_2\text{OH}]_t \approx [{}^{\bullet}\text{C}(\text{CH}_3)_2\text{OH}]_0 \exp(-k_{\text{obs}}t) \quad (\text{A1.7})$$

**Supporting Information Available:** Figures giving additional TRVIS kinetics and HPLC spectra and an Appendix giving the Beer–Lambert Law for competitively absorbing species. This material is available free of charge via the Internet at <http://pubs.acs.org>.

## References and Notes

- O'Neill, C.; Hawkes, F. R.; Hawkes, D. L.; Lourenço, N. D.; Pinheiro, H. M.; Delée, W. *J. Chem. Technol. Biotechnol.* **1999**, *74*, 1009.
- Hepel, M.; Luo, J. *Electrochim. Acta* **2001**, *47*, 729.
- Bessekhoud, Y.; Chaoui, N.; Trzpit, M.; Ghazzal, N.; Robert, D.; Weber, J. V. *J. Photochem. Photobiol. A* **2006**, *183*, 218.
- Bianco Prevot, A.; Fabbri, D.; Pramauro, E.; Baiocchi, C.; Medana, C. *J. Chromatogr. A* **2008**, *1202*, 145.
- Batchelor, S. N. *New J. Chem.* **2004**, *28*, 1200.
- Nadtochenko, V.; Kiwi, J. *J. Chem. Soc., Faraday Trans.* **1997**, *93*, 2373.
- Lorimer, J. P.; Mason, T. J.; Plattes, M.; Phull, S. S.; Walton, D. J. *Pure Appl. Chem.* **2001**, *73*, 1957.
- Lin, S. H.; Peng, C. F. *Water Res.* **1994**, *28*, 277.
- Gutierrez, M. C.; Crespi, M. J. *Soc. Dyers Colour.* **1999**, *115*, 342.
- Fernandes, A.; Morão, A.; Magrinho, M.; Lopes, A.; Gonçalves, I. *Dyes Pigm.* **2004**, *61*, 287.
- Şolpan, D.; Güven, O.; Takács, E.; Wojnárovits, L.; Dajka, K. *Radiat. Phys. Chem.* **2003**, *67*, 531.
- El-Assy, N. B.; Abdel-Rehim, F.; Abdel-Gawad, A. S.; Abdel-Fattah, A. A. *J. Radioanal. Nucl. Chem.* **1992**, *157*, 133.
- Zhang, S.-J.; Yu, H.-Q.; Li, Q.-R. *Chemosphere* **2005**, *61*, 1003.
- Bragger, J. L.; Lloyd, A. W.; Soozandehfar, S. H.; Bloomfield, S. F.; Marriott, C.; Martin, G. P. *Int. J. Pharm.* **1997**, *157*, 61.
- Coughlin, M. F.; Kinkle, B. K.; Bishop, P. L. *Chemosphere* **2002**, *46*, 11.
- Kudlich, M.; Bishop, P. L.; Knackmuss, H. J.; Stolz, A. *Appl. Microbiol. Biotechnol.* **1996**, *46*, 597.
- López, C.; Valade, A.-G.; Combourieu, B.; Mielgo, I.; Bouchon, B.; Lema, J. M. *Anal. Biochem.* **2004**, *335*, 135.
- Lucas, M. S.; Peres, J. A. *Dyes Pigm.* **2006**, *71*, 236.
- Oakes, J.; Gratton, P. *J. Chem. Soc., Perkin Trans. 2* **1998**, 2201.
- Oakes, J.; Gratton, P. *J. Chem. Soc., Perkin Trans. 2* **1998**, 2563.
- Oakes, J.; Gratton, P.; Clark, R.; Wilkes, I. *J. Chem. Soc., Perkin Trans. 2* **1998**, 2569.
- Hodges, G. R.; Lindsay Smith, J. R.; Oakes, J. *J. Chem. Soc., Perkin Trans. 2* **1999**, 1943.
- Brown, M. A.; DeVito, S. C. *Crit. Rev. Environ. Sci. Technol.* **1993**, *23*, 249.
- Hon, D. N.-S. *J. Polym. Sci.: Polym. Chem. Ed.* **1979**, *17*, 441.
- Sirbiladze, K. J.; Rusznák, I.; Víg, A.; Krichevskiy, G. E.; Anysimova, O. M.; Anysimov, V. M. *Dyes Pigm.* **1992**, *19*, 235.
- Rémi, E.; Horváth, O.; Víg, A.; Rockenbauer, A.; Korecz, L.; Aranyosi, P.; Rusznák, I. *Radiat. Phys. Chem.* **1996**, *47*, 461.
- Yadav, P.; Rao, B. S. M.; Batchelor, S. N.; O'Neill, P. *J. Phys. Chem. A* **2005**, *109*, 2039.
- Hunt, P.; Worrall, D. R.; Wilkinson, F.; Batchelor, S. N. *Photochem. Photobiol. Sci.* **2003**, *2*, 518.
- Hunt, P.; Worrall, D. R.; Wilkinson, F.; Batchelor, S. N. *J. Am. Chem. Soc.* **2002**, *124*, 8532.
- Sharma, K. K.; O'Neill, P.; Oakes, J.; Batchelor, S. N.; Rao, B. S. M. *J. Phys. Chem. A* **2003**, *107*, 7619.
- Sharma, K. K.; Rao, B. S. M.; Mohan, H.; Mittal, J. P.; Oakes, J.; O'Neill, P. *J. Phys. Chem. A* **2002**, *106*, 2915.
- Abbott, L. C.; Batchelor, S. N.; Oakes, J.; Gilbert, B. C.; Whitwood, A. C.; Lindsay Smith, J. R.; Moore, J. N. *J. Phys. Chem. A* **2005**, *109*, 2894.
- Vinodgopal, K.; Kamat, P. V. *J. Photochem. Photobiol. A* **1994**, *83*, 141.
- Coen, J. J. F.; Smith, A. T.; Candeias, L. P.; Oakes, J. *J. Chem. Soc., Perkin Trans. 2* **2001**, 2125.
- Bandara, J.; Kiwi, J. *New J. Chem.* **1999**, *23*, 717.
- Jockusch, S.; Landis, M. S.; Freiermuth, B.; Turro, N. J. *Macromolecules* **2001**, *34*, 1619.
- Abbott, L. C.; MacFaul, P.; Jansen, L.; Oakes, J.; Lindsay Smith, J. R.; Moore, J. N. *Dyes Pigm.* **2001**, *48*, 49.
- Nelder, J. A.; Mead, R. *Comput. J.* **1965**, *7*, 308.
- Stanoeva, T.; Neshchadin, D.; Gescheidt, G.; Ludvik, J.; Lajoie, B.; Batchelor, S. N. *J. Phys. Chem. A* **2005**, *109*, 11103.

(40) The signal decay at  $\geq 0.5$  s may result, at least in part, from diffusion out of the probe beam.

(41) In principle, experimental conditions could have been altered to obtain pseudo-first-order conditions by either increasing [Orange II]<sub>0</sub> or decreasing [<sup>13</sup>C(CH<sub>3</sub>)<sub>2</sub>OH]<sub>0</sub>, but neither of these changes was practicable. Orange II absorbs appreciably at the laser wavelength of 308 nm, and so higher dye concentrations would have resulted in a larger proportion of the pump photons being absorbed by the dye and screening of the photoinitiator becoming significant (see Appendix SA1, Supporting Information). The alternative method of lowering [<sup>13</sup>C(CH<sub>3</sub>)<sub>2</sub>OH]<sub>0</sub> could have been achieved by using either a lower photoinitiator concentration or a lower laser pump energy, but this would have resulted in a lower peak concentration of the Orange II radical anion that was a priority of this study, and very weak transient absorption at 650 nm.

(42) Abbott, L. C.; Feilden, C. J.; Anderton, C. L.; Moore, J. N. *Appl. Spectrosc.* **2003**, *57*, 960.

(43) *Landolt-Börnstein: Radical Reaction Rates in Liquids*; Springer Verlag: Berlin, 1984.

(44) Neta, P.; Grodowski, J.; Ross, A. B. *J. Phys. Chem. Ref. Data* **1996**, *25*, 709.

(45) Huggenberger, C.; Lipscher, J.; Fischer, H. *J. Phys. Chem.* **1980**, *84*, 3467.

(46) The reaction of ArCO<sup>•</sup> with <sup>13</sup>C(CH<sub>3</sub>)<sub>2</sub>OH may produce either photoinitiator by addition or ArCHO and (CH<sub>3</sub>)<sub>2</sub>CO by disproportionation; step 7 in Scheme 2 does not make a distinction and *k*<sub>7</sub> effectively includes both routes.

(47) Each laser pulse energy results in a different initial concentration of 2-hydroxy-2-propyl radicals, and so the data from eight laser pulse energies could be modelled with eight independent values of [<sup>13</sup>C(CH<sub>3</sub>)<sub>2</sub>OH]<sub>0</sub>; however, the relative values of the eight [<sup>13</sup>C(CH<sub>3</sub>)<sub>2</sub>OH]<sub>0</sub> values are proportional to the eight measured laser pulse energies, and so we used a fixed set of relative scaling values and a single variable parameter. In contrast, the parameters *k*<sub>2</sub>, *k*<sub>3</sub>, and  $\epsilon_{650}(\text{Dye}^{\bullet-})$  do not vary with the laser pulse energy.

(48) A good fit to the concentration-dependent experimental kinetics was obtained by decreasing the value of [<sup>13</sup>C(CH<sub>3</sub>)<sub>2</sub>OH]<sub>0</sub> by ca. 35% from that given in Table 1 (which gave a good fit to the laser pump energy dependent kinetics). This change was required because of optical realignment that changed the pumping efficiency between the two sets of experiments; all of the other parameters in Table 1 are unaffected by this concentration, and their values were kept constant between the two datasets.

(49) Batchelor, S. N.; Shushin, A. I. *J. Phys. Chem. B* **2001**, *105*, 3405.

(50) Batchelor, S. N. *J. Phys. Chem. B* **1999**, *103*, 6700.

(51) Scheuermann, R.; Roduner, E.; Batchelor, S. N. *J. Phys. Chem. B* **2001**, *105*, 11474.

(52) *CRC Handbook of Chemistry and Physics*, 86th ed.; Lide, D. R. Ed.; CRC Press: Boca Raton, FL, 2005.

(53) Kudlich, M.; Hetheridge, M. J.; Knackmuss, H.-J.; Stolz, A. *Environ. Sci. Technol.* **1999**, *33*, 896.

(54) Fiegl, F. *Spot Tests in Organic Analysis*; Elsevier Publishing Company: Amsterdam, 1960.

(55) Li, Q.-M.; Yang, Z.-J. *Spectrochim. Acta, Part A* **2007**, *66*, 656.

(56) Asahi, Y.; Tanaka, M.; Shinozaki, K. *Chem. Pharm. Bull.* **1984**, *32*, 3093.

(57) Troll, W. *J. Biol. Chem.* **1953**, *202*, 479.

(58) Biggs, I. D.; Tedder, J. M. *Tetrahedron* **1978**, *34*, 1377.

(59) Neta, P.; Levanon, H. *J. Phys. Chem.* **1977**, *81*, 2288.

(60) Zielonka, J.; Podsiadły, R.; Czerwińska, M.; Sikora, A.; Sokołowska, J.; Marcinek, A. *J. Photochem. Photobiol. A* **2004**, *163*, 373.

(61) Monti, S.; Flamigni, L. *J. Phys. Chem.* **1986**, *90*, 1179.

(62) Pérez-Urquiza, M.; Beltrán, J. L. *J. Chromatogr. A* **2001**, *917*, 331.

(63) Ma, M.; Johnson, K. E. *J. Electroanal. Chem.* **1993**, *355*, 97.

(64) Irving, C. C. *J. Org. Chem.* **1960**, *25*, 464.

(65) Hart, J. P.; Franklin Smyth, W. *Analyst* **1980**, *105*, 929.

JP9021147